Multibody System Dynamics (2005) 14: 205–224

Friction Models and Stress Recovery Methods in Vehicle Dynamics Modelling

KRZYSZTOF ARCZEWSKI and JANUSZ FRĄCZEK
Institute of Aeronautics and Applied Mechanics, Warsaw University of Technology, Nowowiejska 24,00-665 Warsaw, Poland; E-mail: krisarcz@meil.pw.edu.pl

(Received 1 September 2003; accepted in revised form 23 July 2004)

Abstract. This paper presents two examples of calculations for vehicles with flexible bodies by using mixed multibody and finite element methods. The first example deals with dynamics computations for a bimodal train with a flexible cistern, whereas the second example concerns the dynamics calculations for the PW-6 glider. In the first example, the influence of the chosen friction model on the train dynamics calculations results was discussed. The second example presents several methods of stress calculations and a comparison of results. The achieved conclusions may be used as suggestions towards a modelling method choice for a given problem. Both issues being discussed are of great importance in dynamics of flexible multibody systems modelling practice and durability assessment.

In both examples, the kinematics of the system was presented in absolute coordinates, the motion equations in the DAE form, and the reduction of the number of degrees of freedom was achieved by means of the Craig–Bampton (CB) method.

Keywords: dynamics, vehicle, multibody, flexibility, friction, stress

1. Introduction

The design of new railroad vehicles and airborn structures requires simulation research. In these experiments, techniques based on Multibody Systems (MBS) and Finite Element Methods (FEM) are widely used. The simplest multibody vehicle models are composed of rigid bodies only, whereas the more complex models are designed with the assumptions of free rotation and translation of the bodies as well as their susceptibility to deformations, with geometric and material nonlinearities.

Lately, a broad range of models, in which the multibody system is composed of both rigid and flexible bodies, is used. Flexible bodies are being assumed to undergo deformations in linear strain–stress and strain–displacement regimes. Motion of the flexible body is characterized by large motion of a body reference frame and a displacement field relative to the body reference frame [1]. This approach was originally motivated by the assumption of infinitesimal strain and is called the floating-frame approach. Under these assumptions, linear stress–strain relations and linear strain–displacement relations can be used, thus allowing a simple expression for the strain energy of the body. The relative displacement field can then be approximated using a linear FEM or a component mode synthesis (CMS) approach. In this approach, for multibody systems

involving high-speed rotating components, the stress-stiffening effect must often be accounted for although the material is within linear elastic region and displacements are small. Many formulations that extend the floating-frame approach to capture such stress-stiffening behaviour have been proposed [2]. Recently, the floating-frame approach has been extended to incorporate large deformation and material nonlinearity [3].

In this paper, two applications of the floating-frame approach algorithm have been presented for modelling the dynamics of two new designs: a prototype of a bimodal train with a flexible cistern during its motion along a curved path and a PW-6 glider during touchdown.

The presentation and discussion of the bimodal train dynamics test results is focused on the influence of several friction models in the kinematic pairs on the solution. Three different dry friction models most commonly used in practical calculations and commercial software packages have been assumed.

During the study of the PW-6 glider dynamics, several methods of reduced stress estimation based on force and displacement calculations have been used. Stresses are used not only for the estimation of the structure strength, but also for structure durability tests. Also, the influence of the motion equation integration method in formulations with different indexes upon the solution has been evaluated.

Obtained conclusions and suggestions may be used as pointers towards the proper choice of friction modelling and stress estimation methods.

The paper has been structured as follows: at first, techniques for modelling friction forces and solving motion equations dependent on a given friction model have been presented. Secondly, the procedure of flexible systems modelling and stress calculation methods have been explained. The following chapters present details of the bimodal train and glider models as well as the results obtained depending on the chosen friction model and stress estimation method. Finally, conclusions based on result comparisons have been pointed out.

2. Multibody Dynamics with Friction

Equations of motion of a rigid multibody system without friction can be written with the use of absolute coordinates in index-3 formulation [4, 5]:

$$\begin{cases} \dot{\mathbf{q}} - \mathbf{v} = \mathbf{0} \\ \mathbf{M}(\mathbf{q})\dot{\mathbf{v}} = -\boldsymbol{\Phi}_{\mathbf{q}}^{T}(\mathbf{q}, t)\boldsymbol{\lambda} + \mathbf{Q}(\mathbf{q}, \mathbf{v}, t) \\ \boldsymbol{\Phi}(\mathbf{q}, t) = \mathbf{0} \end{cases} \tag{1}$$

where $\boldsymbol{\lambda}$ represents a vector of Lagrange multipliers responsible for the values of the reaction forces at the constraints, $\mathbf{Q}$ is a vector of generalized forces and $\mathbf{M}$ is the inertia matrix.

Equation (1) can be integrated using one of the generally available numerical methods [6], most often based on the BDF or IRK schemes [7].

According to the way of friction force modelling, the set of equations in the form (1) can be modified to a form which involves static and dynamic friction forces. If the friction force model assumes the friction to have an external force characteristic (which depends on the reaction forces in the kinematic pairs), the motion Equations (1) can be written in the form:

$$\begin{cases} \mathbf{M}\dot{\mathbf{v}} = -\boldsymbol{\Phi}_{\mathbf{q}}^{T}\boldsymbol{\lambda} + \mathbf{Q} + \mathbf{Q}_T(\boldsymbol{\lambda}) \\ \boldsymbol{\Phi}(\mathbf{q}, t) = \mathbf{0} \end{cases} \tag{2}$$

The $\mathbf{Q}_T(\boldsymbol{\lambda})$ notation emphasises the fact that the friction forces depend explicitly on the Lagrange multipliers.

The friction model can also be constructed on the basis of the assumption that static friction is the result of additional constraints, whereas kinetic friction is treated as external force [8]. In order for Equation (2) to include the additional constraints coming from static friction, it must be further modified:

$$\begin{cases} \mathbf{M}\dot{\mathbf{v}} = -\boldsymbol{\Phi}_{\mathbf{q}}^{T}\boldsymbol{\lambda} - (\boldsymbol{\Phi}_T)_{\mathbf{q}}^{T}\boldsymbol{\lambda}_T + \mathbf{Q} + \mathbf{Q}_T(\boldsymbol{\lambda}, \boldsymbol{\lambda}_T) \\ \boldsymbol{\Phi} = \mathbf{0} \\ \boldsymbol{\Phi}_T = \mathbf{0} \end{cases} \tag{3}$$

where the multipliers $\boldsymbol{\lambda}_T$ correspond to the static friction based constraints. Equation (3) can be written in the index-1 formulation:

$$\begin{bmatrix} \mathbf{M} & \bar{\boldsymbol{\Phi}}_{\mathbf{q}}^{T} \\ \bar{\boldsymbol{\Phi}}_{\mathbf{q}} & \mathbf{0} \end{bmatrix} \begin{bmatrix} \ddot{\mathbf{q}} \\ \bar{\boldsymbol{\lambda}} \end{bmatrix} = \begin{bmatrix} \mathbf{Q} + \mathbf{Q}_T(\bar{\boldsymbol{\lambda}}) \\ \bar{\boldsymbol{\Gamma}} \end{bmatrix}, \quad \text{where } \bar{\boldsymbol{\Phi}} = \begin{bmatrix} \boldsymbol{\Phi} \\ \boldsymbol{\Phi}_T \end{bmatrix}, \quad \text{and } \bar{\boldsymbol{\lambda}} = \begin{bmatrix} \boldsymbol{\lambda} \\ \boldsymbol{\lambda}_T \end{bmatrix} \tag{4}$$

To describe the friction in kinematic pairs, friction models based on the following assumptions are generally used [9]:

1. Friction forces are described by one of the models from *a* to *c* (with discontinuity) Figure 1
2. The friction force depends on the relative velocity, as described in Figure 1d
3. In the neighbourhood of relative velocity equals zero, friction force depends on the relative velocity and microslip (Figure 2). The friction outside of that zone depends on relative velocity [10] (according to model 1c).

If the friction force is being modelled according to Figure 1b, the static friction can be described as a reaction coming from additional constraints [8] and the kinetic friction as an external force proportional to the relative velocity. In such a

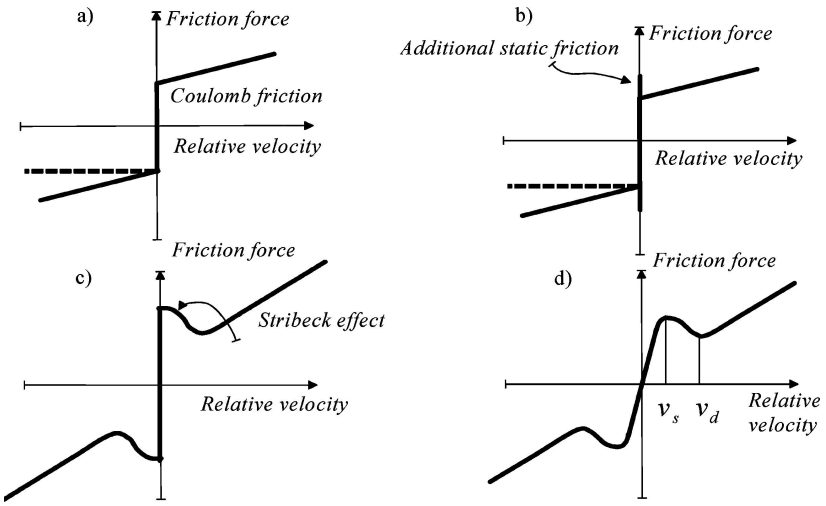

Figure 1. Different models of friction used in multibody modelling practice: (a) Coulomb model, (b) Coulomb friction + stiction + viscotic, (c) Coulomb friction + Stribeck effect + stiction + viscotic friction, (d) simplified model.

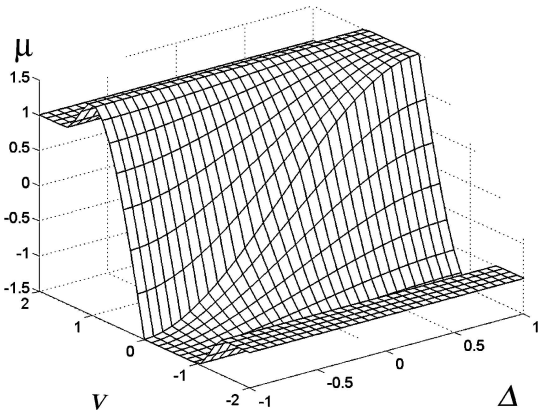

Figure 2. Joint friction model with microslip Δ and relative velocity v[10].

case, equations in the form (3) or (4) are being used, with an iterative solution [11] and constraint stabilization.

In case of the friction force according to Figure 1d, the model is useful mainly for modelling of the kinetic friction; the static friction phase is described only in a simplified manner. The model from Figure 2 assumes that a microslip occurs during the static friction phase, thus it can be used in a relative motion rest phase between two bodies in a kinematic pair. If the friction force is being modelled according to Figure 1d and Figure 2, equations of motion in the form (2) or (4) can be used.

The evaluation of the influence of different friction models shown in Figure 1 and 2 is important in modelling practice, since friction substantially influences the

results and computational complexity. It should also be noted that the models from Figure 1b and Figure 2 comprise the default method for modelling friction forces in two oldest and most widely used commercial software packages [8, 10].

3. Floating-Frame Approach in Flexible Multibody Dynamics: Stress Recovery Methods

If a system of rigid bodies is modelled by means of the floating-frame approach in the range of small deformations, the equations of motion can be written as follows [1]:

$$\begin{bmatrix} \mathbf{m}_{SS} & \mathbf{m}_{Sf} \\ \mathbf{m}_{fS} & \mathbf{m}_{ff} \end{bmatrix} \begin{bmatrix} \ddot{\mathbf{q}}_S \\ \ddot{\mathbf{q}}_f \end{bmatrix} + \begin{bmatrix} \mathbf{0} & \mathbf{0} \\ \mathbf{0} & \mathbf{D}_{ff} \end{bmatrix} \begin{bmatrix} \dot{\mathbf{q}}_S \\ \dot{\mathbf{q}}_f \end{bmatrix} + \begin{bmatrix} \mathbf{0} & \mathbf{0} \\ \mathbf{0} & \mathbf{K}_{ff} \end{bmatrix} \begin{bmatrix} \mathbf{q}_S \\ \mathbf{q}_f \end{bmatrix} = \begin{bmatrix} (\mathbf{Q}_z)_S \\ (\mathbf{Q}_z)_f \end{bmatrix} + \begin{bmatrix} (\mathbf{Q}_v)_S \\ (\mathbf{Q}_v)_f \end{bmatrix} - \mathbf{\Phi}_{\mathbf{q}}^T \boldsymbol{\lambda} \tag{5}$$

where: $\mathbf{\Phi}_{\mathbf{q}}^T \boldsymbol{\lambda}$ – reaction force vector with Lagrange multipliers, $\mathbf{Q}_z$– vector of external forces applied to a flexible body, $\mathbf{Q}_v$– vector of centrifugal, Coriolis and other forces resulting from differentiation of the kinetic energy with respect to time and each of the coordinates. The above matrices can be obtained by means of classical FEM algorithms used in linear range.

To reduce the number of degrees of freedom, the system of Equation (5) is usually written in the form:

$$\begin{bmatrix} \mathbf{m}_{SS} & \mathbf{m}_{Sf}\mathbf{\Psi} \\ \mathbf{\Psi}^T\mathbf{m}_{fS} & \mathbf{I} \end{bmatrix} \begin{bmatrix} \ddot{\mathbf{q}}_S \\ \ddot{\mathbf{p}} \end{bmatrix} + \begin{bmatrix} \mathbf{0} & \mathbf{0} \\ \mathbf{0} & \mathbf{d} \end{bmatrix} \begin{bmatrix} \dot{\mathbf{q}}_S \\ \dot{\mathbf{p}} \end{bmatrix} + \begin{bmatrix} \mathbf{0} & \mathbf{0} \\ \mathbf{0} & \Omega \end{bmatrix} \begin{bmatrix} \mathbf{q}_S \\ \mathbf{p} \end{bmatrix} = \begin{bmatrix} (\mathbf{Q}_z)_S \\ \mathbf{\Psi}^T(\mathbf{Q}_z)_f \end{bmatrix} + \begin{bmatrix} (\mathbf{Q}_v)_S \\ \mathbf{\Psi}^T(\mathbf{Q}_v)_f \end{bmatrix} - \begin{bmatrix} \mathbf{\Phi}_{\mathbf{q}_S}^T \\ \mathbf{\Psi}^T\mathbf{\Phi}_{\mathbf{q}_f}^T \end{bmatrix} \boldsymbol{\lambda} \tag{6}$$

The matrix $\mathbf{\Psi}$ can be obtained through different modal synthesis techniques [12]. The elastic deformations of all degrees of freedom are approximated by a linear combination of suitable modes. The component modes contain the static and dynamic behaviour of the structure and they consist of two families of modes: constraints modes and normal modes. In order to get a decoupled set of modes the constraint modes and normal modes are often transformed into a set of orthogonalised component modes [12]; in consequence it is not possible to distinguish between pure static and pure dynamic modes.

It should be pointed out, that the inertia matrix in (6) is a function of a few invariant matrices [1]. Through omitting or including some of them it is possible to control the analysis type and the numerical complexity.

According to the size of displacements or forces obtained after integration of the Equation (6), the stresses in flexible bodies can be estimated. The values of

the obtained stresses can vary significantly depending on the calculation method. Stresses can be estimated by means of the following methods [13–16]:

A. Rigid body stress recovery methods (force based),
B. Flexible body stress recovery – force based with different support sets,
C. Flexible body stress recovery – force based – so-called inertia relief method [13],
D. By combining the modal stress tensor and modal coordinates in Component Mode Synthesis [12, 13, 17].
E. Deformation-based stress recovery [13–15].

Stress calculations are essential for body strength evaluation. The effectiveness and precision of stress calculations plays a major role in the evaluation of system strength and durability.

The issue of stress estimation evaluation for different estimation methods will be discussed on the basis of the PW-6 glider.

4. Floating-Frame Approach in Flexible Bimodal Train Modelling – Comparison of Friction Models

4.1. BIMODAL TRAIN

The bimodal train is an example of combined (rail and road) bimodal transport vehicle, based on a prototype constructed in Poznań, Poland in the middle nineties [18]. The model of the bimodal train was presented [19] such that the effect of flexibility of the cistern was neglected and with simplified model of friction. The three-unit prototype train, with all three-car bodies modelled as rigid, is shown in Figure 3.

The lack of information concerning the dynamical behaviour of the bimodal train with flexible cisterns was the motivation for modelling and investigation of the train on the straight and curved track. However, from the point of view of general multibody modelling, results obtained with different friction models can be interesting and will be discussed here.

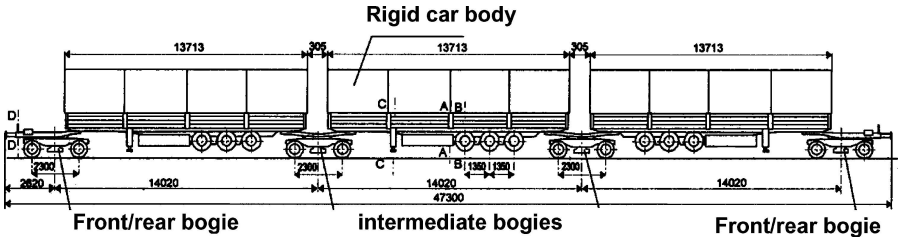

Figure 3. Scheme of the Polish three-unit prototype bimodal train, *Courtesy of* '*Research Institute of Rolling-Stock Industry in Poznań*'.

4.2. THE DETAILS OF THE PROTOTYPE DESIGN

Each car body of the train is equipped [18, 19] with its own carrier structure, which results in the elimination of railway frames. The main parts of the train are bogies, car bodies and adapters. Adapters are the light frames equipped with special locks necessary to connect car bodies to bogies. The prototype of the bimodal bogie, shown in the Figure 3 is based on the standard Y25 freight railway bogie (with some small differences).

Each of the bimodal bogies possesses a swing bolster (Figure 4), which can move laterally. In Figure 4, the intermediate bogie, which connects two adjacent car bodies, is shown. The side support 3 and adapter's locks are used to mount the end of the car body on the bogie frame by the swing bolster. Vertical load from the car body is transmitted to the adapter by the side support and reaction arm and to the bogie frame with pivots (spherical joints). Side friction blocks 10 and 11 receive the load due to rolling of the car body during the motion of the train. The front and rear bogie of the train (leading and trailing) is designed in the similar way and more details can be found in [18].

The primary suspension of the bogie consists of two nested coil springs and friction damper. The spring characteristics have progressive character i.e. in the lower range of the load magnitude only outer springs are loaded, whereas in the higher range both outer and inner springs work.

The secondary suspension is provided by a swing bolster, connected to the bogie frame by two pairs of hangers. Each bogie has the pivot's nest placed at the centre of

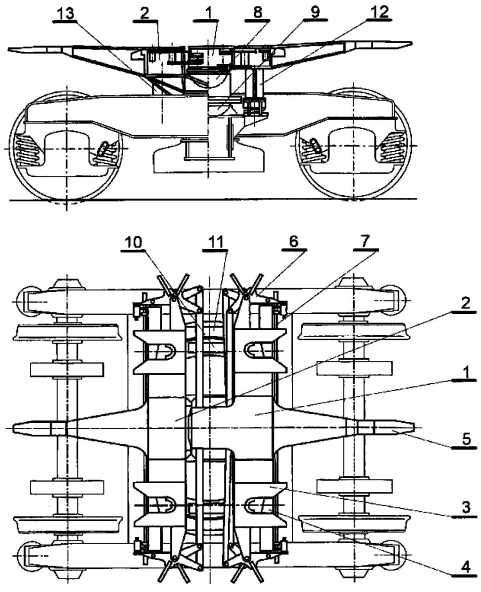

1 – upper adapter,
2 – lower adapter
3 – side support for the car body
4 – lock of the adapter
5 – reaction arm
6 – locking mechanism,
7 – locking mechanism
8 – lower bogie pivot
9 – upper bogie pivot
10 – side friction block
11 – side friction block
12 – adapter's support
13 – adapter's support

Figure 4. Intermediate bogie of the bimodal train, *Courtesy by 'Research Institute of Rolling-Stock Industry', Poznań.*

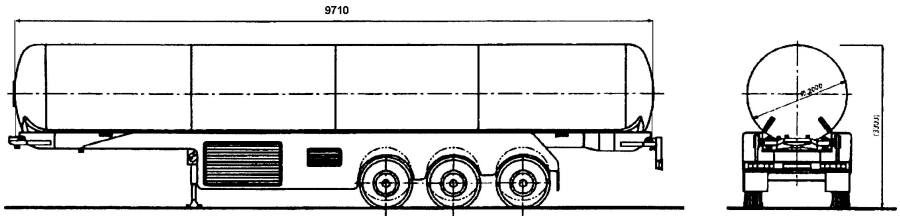

Figure 5. The cistern for liquid transport Courtesy by 'Research Institute of Rolling-Stock Industry', Poznań.

the swing bolster. The spherical pivot and adapter create the unit, which transmits load from the car body to the bogie frame and then to the wheelsets. The train can be assembled with rigid car bodies (Figure 3) or with rigid bodies and flexible cistern. The prototype of the flexible cistern is shown in the Figure 5. In the paper the motion of the three-unit train with one flexible cistern and two rigid bodies was analyzed.

4.3. THE MBS AND FEM MODEL OF THE TRAIN

It was assumed initially that the bimodal train consisted of three units placed on four bogies (Figure 4); two units are rigid and one is a flexible cistern (Figure 5) empty or fully filled with fuel. The multibody model of the intermediate bogie is shown in the Figure 6. All spring and damping elements of suspension are not shown – they were modelled as external nonlinear forces.

The cistern was modelled in a FEM package using shell elements. The meshing of the cistern (Figure 7) and all necessary modal characteristics (including Ritz matrix Ψ) according to relation (6) and CB method with orthogonalisation were prepared in the external commercial FEM code.

The flexible cistern is fixed to the bogie using reaction arms and adapters locks. The kinematical pairs were modelled using interface parts, revolute and translational

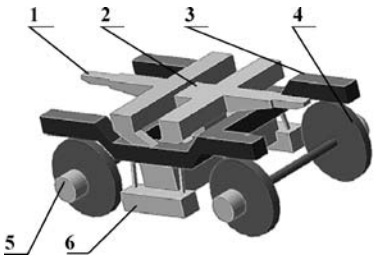

Main parts:
1 – lower adapter, 2- upper adapter, 3 – bogie frame, 4 – wheelsets, 5 – axle boxes, 6- swing bolster

Figure 6. The multibody model of the intermediate bogie – main parts.

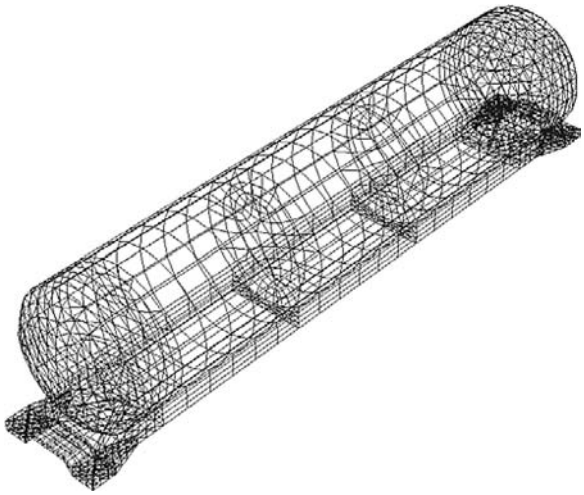

Figure 7. Meshing of the cistern.

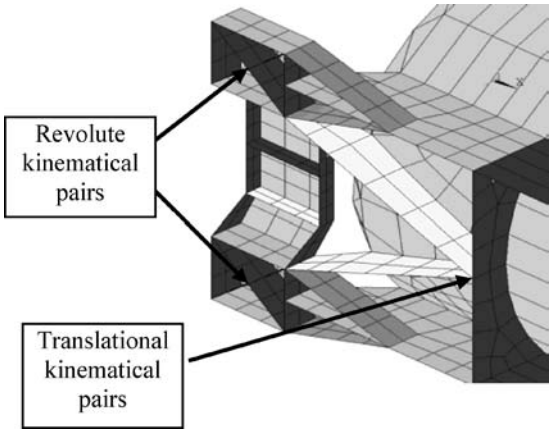

Figure 8. Interface points between cistern and adapters.

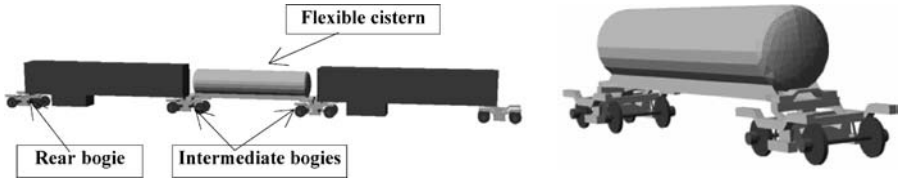

Figure 9. View of the three-unit train and cistern model.

joints (Figures 8 and 9). Boundary DOF's in CB reduction of DOF were chosen in the nodes where kinematical pairs between cistern and adapters were placed. The number of modal coordinates was chosen after many numerical experiments and was equal to 100 in majority of numerical simulation.

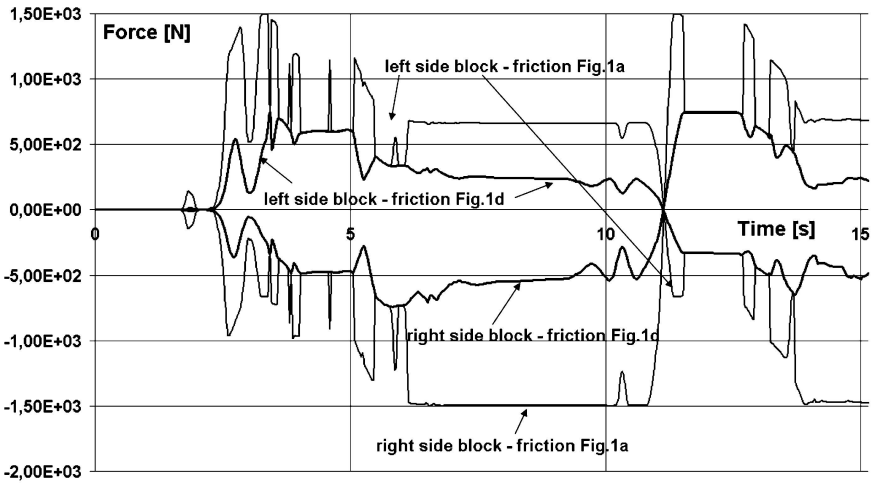

Figure 10. Longitudinal friction forces (x) on the side friction blocks for different friction models (intermediate bogie).

The damping coefficients were taken as 1% of the critical damping for mode shapes with frequencies below 500 Hz, 10% for frequencies between 500 and 1000 Hz, and 100% above.

For introductory simulation of the liquid pressure and dynamics influence, provided the cistern is fully filled (the sloshing effect is neglected), the distributed load of the pressure was translated to node forces. The contact forces between rail and wheels were modelled using nonlinear wheel-rail contact model based on wheel-rail profiles, which allows three-dimensional multi-point contact description [20, 21].

4.4. SIMULATION RESULTS: INFLUENCE OF THE FRICTION MODEL ON CALCULATION RESULTS

The detailed investigations of the train's dynamics require an evaluation of the influence of different model parameters on the train's motion i.e. trajectory parameters (curvatures, cant angles, irregularities), stiffness and suspension damping, etc. From the correctness of the model design process and the application of the calculation method, the evaluation of the influence of different models on simulation results is necessary. It is well known that the friction model is particularly uncertain. For this reason numerous simulations were performed using different friction models presented in Section 2. The examples of the results obtained are presented below.

The Figure 10 shows the longitudinal friction forces on the side blocks of the lower adapter of the bimodal train obtained from calculations of two different friction force modelling variants. In the first variant it was assumed that the friction

forces act according to relations presented in Figure 1a, however with a narrow passing zone and with no distinction between static and kinetic friction (the static friction coefficient is equal to the kinetic friction coefficient). In the second simulation the friction model presented in Figure 1d was chosen with the assumption that the static friction is greater than kinetic friction and the passing zone appears accordingly with Stribeck's effect (10^{-5} m/s velocity corresponding to the maximum static friction was assumed). Numerous stick-slips are visible in the case of a model with a static friction zone. It is possible to verify, by means of a numerical experiment, that applying a wider passing zone (smoother variation process) the number of stick-slips decreases.

The consequence of changing the friction model is the several times greater tangential force on the side blocks obtained in some phases of the motion. It is worth noting that the accuracy of parameter estimation defining friction in vehicles is rather low.

The case presented in Figure 11 deals with the modelling of friction in the kinematical pairs in the upper bogie pivot (spherical kinematical pair). The first variant of the model was built with the assumption that the friction torques in the upper bogie pivot in the lateral and longitudinal direction are negligible. The product of friction coefficient and the radius of the upper bogie pivot are estimated from rough experimental measurements. The model from Figure 1d was chosen. In the second calculation variant the friction was modelled according to Figure 2.

The differences in vertical component (along the z axis) of torque are substantially greater, especially near the zero value of relative velocity. It is important that a considerable longtitudinal torque component appears in the second variant, the influence of which on the train's dynamics cannot be neglected. It is to be expected that the friction model, applied in the first variant, requires verification.

Among another simulation results some results allow estimating the train's safety. From that point of view, the relation between lateral and vertical forces

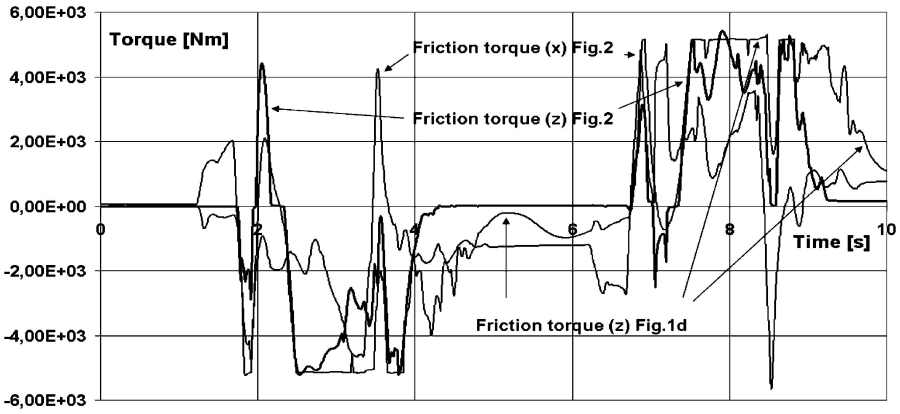

Figure 11. Friction torques in bogie pivot for different friction models (Figure 1d and Figure 2).

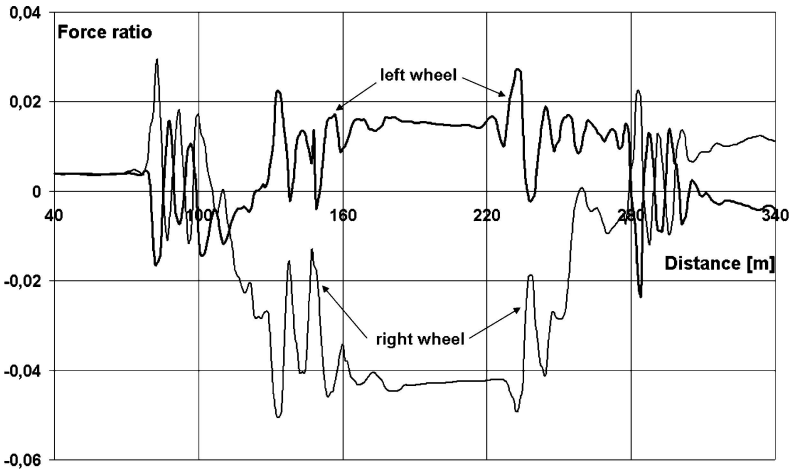

Figure 12. Lateral to vertical forces ratio on the front bogie wheels.

on the wheels of the front bogie is crucial. For the freight bogies the Nadal's criterion is applied, defining sensitivity of the car to derailment. According to this criterion the quotient of the forces cannot exceed 1.2. The Figure 12 shows the relation between lateral and vertical forces obtained from calculations for both wheels of the front bogie. The maximum value of the force quotient is considerably lower than the limit value. To evaluate the influence of the model parameters on the simulations results, calculations with different friction models were performed and similar results to those presented in Figure 12 were obtained.

It should be pointed out that results presented in the Section 4 were obtained using DAE integration algorithms based on BDF schemes for Equations (1) to (4) and implemented in [21].

5. The Analysis of the PW-6 Glider Dynamics: Comparison of the Stress Estimation Methods

5.1. PW-6 GLIDER

The PW-6 glider [22] was designed and built at the Warsaw University of Technology, Faculty of Power and Aeronautical Engineering. The PW-6 is a two-seat tandem mid-wing monoplane glider– Figure 13.

The landing gear of the PW-6 is fixed to the fuselage and consists of the front and rear part. It is equipped with a drum brake (Figure 13). The dimensions of the PW-6 glider are:

– fuselage length – 7.85 m;
– fuselage height – 0.64 m;
– wingspan – 16 m.

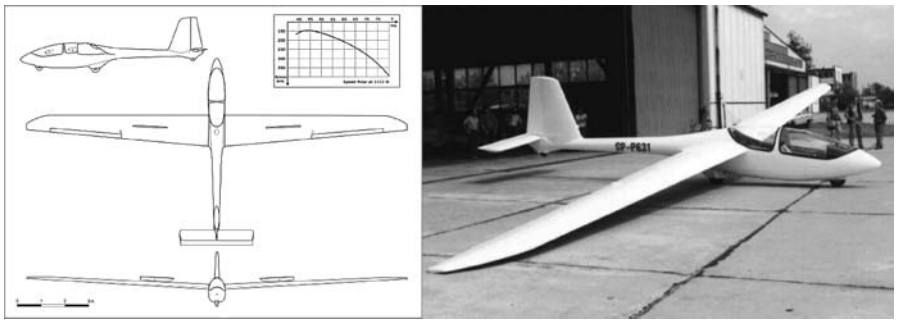

Figure 13. PW-6 glider – technical details and general view.

5.2. THE MBS AND FEM MODEL OF THE PW-6 GLIDER

To perform the analysis of the glider's dynamics during the landing manoeuvre, a calculation model was developed based on the multibody method. The floating-frame approach algorithm presented in Section 3 was used. In the FE models employed here, the tacit assumption has been made that idealized, single-grid connections between system components can be made. Within the different calculation variants, a comparison of different methods of stress estimation was performed. The obtained results can be used as a suggestion and comment towards the evaluation of these methods.

The glider's fuselage (Figure 14) was modelled in an FEM software environment [23, 24] using quad-shell elements (2125 elements) and rigid-body elements (RBE)

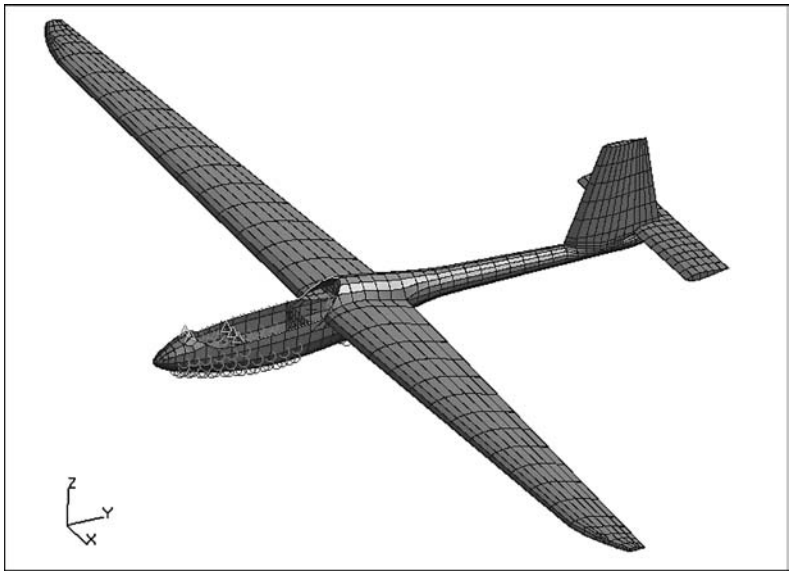

Figure 14. FEM model of the PW-6 glider fuselage.

to model external fixing points. The model of the front and main (rear) suspension was prepared using the multibody method.

The calculations of the glider's dynamics (kinematical parameters) were performed using both the multibody method and floating-frame approach. FEM was used to estimate stresses using various methods.

The calculations were performed with the simplifying assumption that the material of the fuselage is duralumin. In fact, the fuselage of the PW-6 glider is made of glass/epoxy composite. For this material the floating-frame approach methods could not be applied (Section 3).

5.3. THE FRONT AND REAR-SUSPENSION MODEL: MODELS OF PILOTS

The front suspension consists only of the front wheel, which is directly fixed to the glider's fuselage. The rear suspension consists of the main wheel, bellcrank and the shock absorber, which are connected with each other and with the fuselage by means of kinematical pairs (Figure 15). The simplified models of the two pilots are added to the glider's model with front and rear suspensions (Figure 15). It was assumed that during the flight and landing manoeuvre the pilots are not in motion.

5.4. THE DYNAMIC ANALYSIS OF THE LANDING MANOEUVRE

The physical phenomenon considered in this study is the dynamics of the PW-6 glider landing manoeuvre. The most frequent landing variant was tested – landing on the main wheel with the front wheel just above the ground. During the landing approach phase, the glider should have the proper rate of descent, which is defined in international regulations concerning the design and operation of JAR-22 gliders – the velocity amounts to 1.5 m/s. In the study, the rate of descent was established at 1.955m/s in order to test the behaviour of the glider. The total simulation time of the glider's landing manoeuvre equals 2 s. The gear-ground contact phase lasts for approximately 1.8 s.

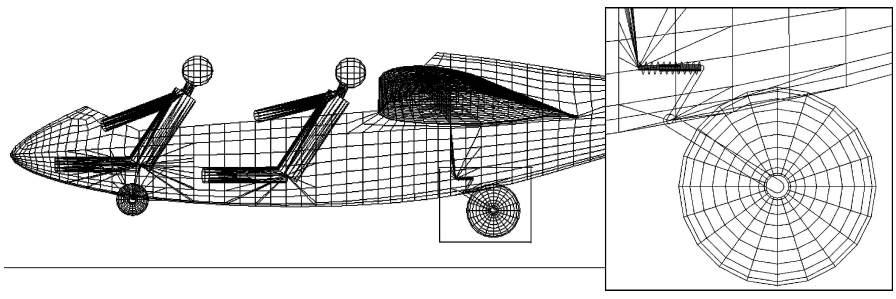

Figure 15. Model of rear suspension and simplified rigid body model of pilots.

5.5. STRESS RECOVERY METHODS

To estimate stresses in selected parts of the glider's structure, the following evaluation methods were used:

A. Rigid body stress recovery – force based. Neglecting body deformations, it is possible to calculate forces and accelerations of the studied system, and then the stresses using FEM software, with a statically determinated support.
B. Flexible body stress recovery – force based. The estimation of stresses is performed as above but all the bodies are treated as flexible. Then, using FEM software, the static calculations of the system, with statically determinated supports, were performed. Calculated reaction forces are used to evaluate the correctness of computations (force values should be numerically close to 0).
C. Flexible body stress recovery – force based – inertia relief [13]. Basing on the inertia and gravity forces calculated in a multibody analysis, the system is kept in kinetostatic equilibrium.
D. Modal stress recovery. During the modal basis generation phase in the FEM code, additional information can be also precomputed for lately combining the modal coordinates to the FE stresses. This so-called modal stress tensor identifies the stress component associated with each orthogonalized mode shape. All calculations for stress evaluations are carried out in MBS software.
E. Deformation-based stress recovery. Stresses are calculated on the basis of node displacements obtained from calculations in MBS software. This can be done using FEM analysis by stress estimation based on node displacement in consecutive time steps.

The methods mentioned above were used for stress evaluation of different elements of the glider in many different places of the fuselage.

The further part of this study presents selected results of stress analysis for selected time interval in the neighbourhood of two selected nodes – node 1072 and node 915 (Figure 16). Node 1072 is located in the place on the wing of the glider where high level of stresses is observed (Figure 17b, c). Node 915 is placed on the rear wall of the cabin of the glider in the area of moderate stresses (Figure 18b, c).

5.6. RESULTS

The comparisons of different stress recovery methods in the form of stress trajectories calculated in the time interval < 0.19 s, 0.5 s $>$ in nodes 1072 and 915 with methods A through E are presented in Figure 17a and Figure 18a, respectively.

Stress distributions corresponding to time 0.36 s (maximal values of stresses obtained using methods D and E) for force-based method and deformation-based method, respectively are shown in the Figure 17b, c and in the Figure 18 b,c.

In the area of stress concentration (Figure 17b, c) in the first phase of landing (approximately from 0.2 to 0.3 s) the representation of the flexible structure as rigid

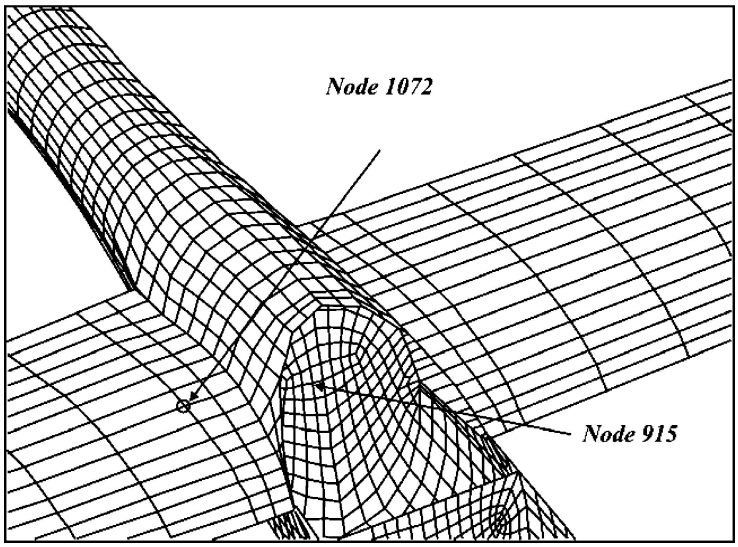

Figure 16. Location of nodes 1072 (high-stresses area) and 915 (moderate-stresses area).

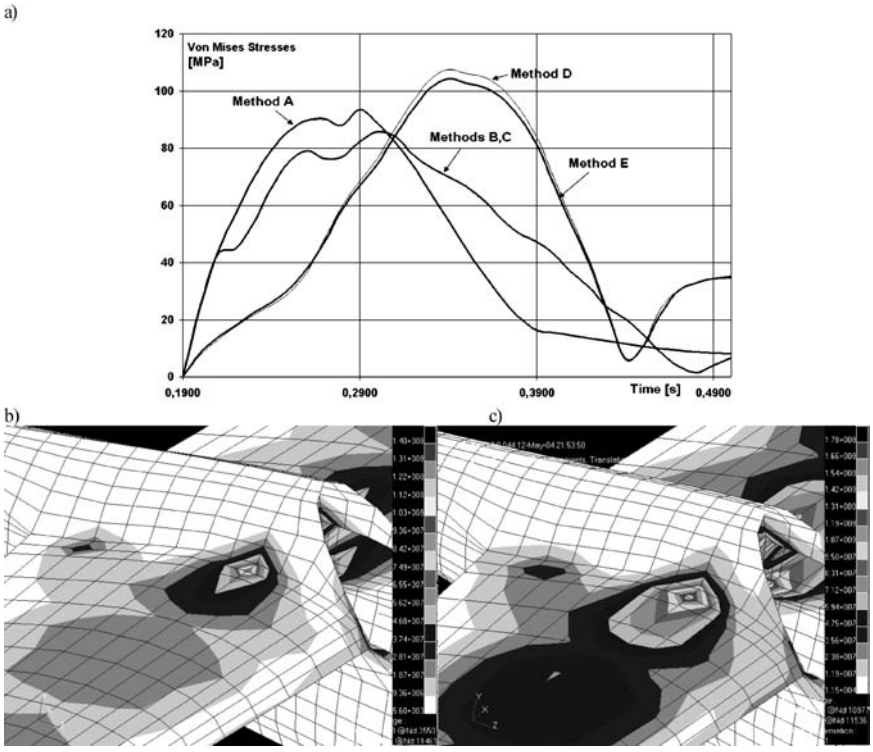

Figure 17. (a) Stress trajectories in node 1072, (b) Stress distribution in the neighbourhood of the node 1072 at time 0.36 s obtained with method C, (c) Stress distribution in the neighbourhood of the node 1072 at time 0.36 s obtained with method E.

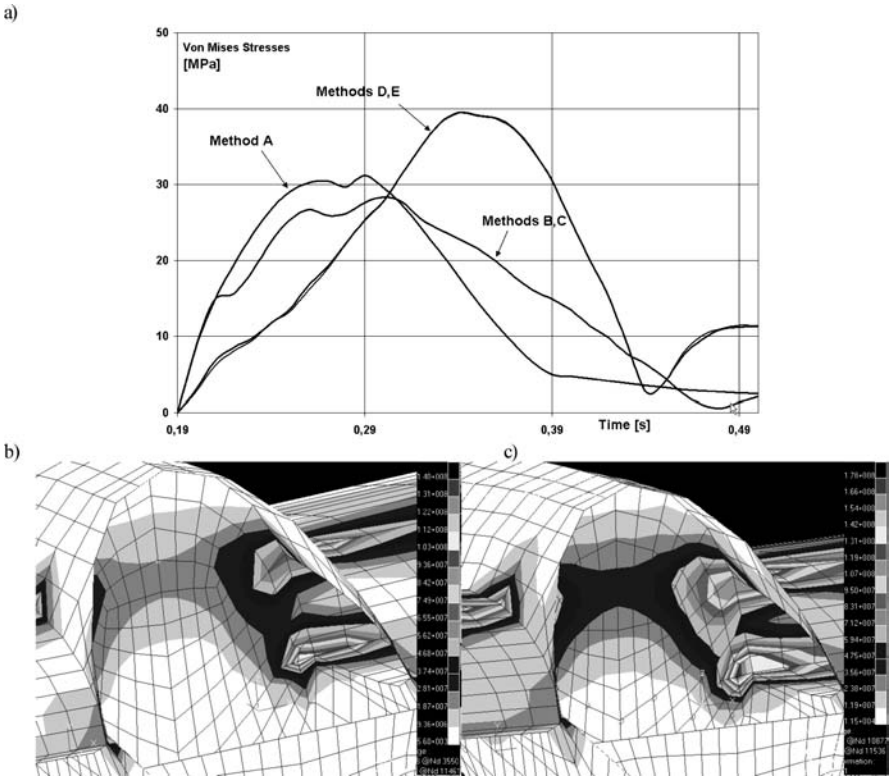

Figure 18. (a) Stress trajectories in node 915, (b) Stress distribution in the neighbourhood of the node 915 at time 0.36 s obtained with method C, (c) Stress distribution in the neighbourhood of the node 915 at time 0.36 s obtained with method E.

(method A) as well as the force methods for stress recovery (B, C) lead to stress overestimation in comparison with displacement and modal methods (D, E). In the second phase (from 0.3 to 0.5 s), the displacement methods give significantly higher stress levels. However, the maximal values of stresses calculated with force-based methods in this time interval are underestimated in comparison with methods D and E.

Similar situation is observed in case of stress evaluation in the node 915 (moderate stress area). However, the relative discrepancy between maximal values is greater than in the previous case and climbs to 30%. In case of strength evaluation or durability analysis such difference can make several analyses useless.

Significant differences between stresses calculated using different methods are also observed at time 0.49 s. The stress levels obtained using methods D and E are significantly greater than in force-based methods. These differences are attributable to the fact, that the modal- and displacement-stress recovery methods include the modal acceleration effects in the inertial terms of the system differential equations, which the force-based approach does not.

Finally, it should be pointed out that in method B several variants of statically determined supports have always been investigated.

6. Conclusions

The dynamic analysis of a bimodal train with flexible bodies achieved by means of the free-floating approach enabled the derivation of several train characteristics invaluable during the design phase. On the basis of the assessment of the influence of friction models on simulation results, it can be stated that:

1. The friction model in which static friction is modelled as a reaction of additional constraints [11] is similar to the model originally proposed by Coulomb. It is, however, troublesome in its numerical implementation (it requires the detection of moments in which switching between friction types occurs). Greater difficulties emerge also during integration of the DAE equations of motion.
2. Friction models from Figures 1(a–d) assume that the friction depends only on relative velocity. Therefore, in the kinetic friction regime, they are similar to the Coulomb- Amontons model. In the model from Figure 2, it is being assumed that static fiction is being accompanied by a microslip and therefore it is a function both of relative velocity and microslip itself.
3. The numerical implementation of the model from Figure 2 is simple and adequate for modelling of static friction. The model confirms experimental results showing that static friction is accompanied by a microslip. All friction models shown are so-called static friction models [9].
4. Differences in simulation results for different friction models and equal coefficients ranged up to several dozen percent. This implies that it is difficult to obtain a valid friction model without the experimental validation.
5. If friction is being modelled in the contact phase of two bodies where the force directions are not known *a priori*, the implementation of the friction model from Figure 1d is the simplest one, however, the friction is also very crudely approximated in the range of zero relative velocity.

Based on the comparison analysis method used to estimate stresses in the example of the PW-6 glider, it can be stated that:

1. Stress calculations based on several variants of force methods give similar stress values. It should be noted that kinetostatic calculations in this method do not take into account modal accelerations.
2. Values of stresses computed from analysis A (rigid representation of the structure) differ from the remaining values. Rigid representation should only be used if representative flexible structures are not available, or the investigation has proven conclusively that flexible effects are, indeed, negligible.

3. In most practical cases the force-based stress recovery [13] methods underestimate maximal stresses resulting from dynamic loading of the system. It is illustrated for both cases of stress analysis – in node 1072 and in node 915 comparing e.g. methods B and D (Figure 17 and Figure 18).
4. Usually the analysis results based on the displacement and modal methods (methods D, E) differ substantially from the results obtained by means of the force method. It can be therefore concluded that omitting inertia effects resulting from modal accelerations can have a strong influence on the results.
5. It should be pointed out that loads generated from flexible structures for force-based stress recovery are incomplete in that they do not contain the structural acceleration. Depending on the structure and the loading environment to which it is subjected, this can result in critical stresses being underestimated or, in the worst case, missed completely.
6. From the standpoint of completeness and accuracy the methods D and E (modal and displacement based) give more reliable results than any of the force-based approaches.
7. An important aspect of kinetostatic analyses is the proper choice of support sets; in case of complicated objects and phenomena in most cases proper results were obtained using supports based on method C.
8. The integration methods used during the process of solving DAE equations of motion have a strong impact on the result accuracy [6]. In the examples provided, results obtained by means of different integration procedures (stabilized index 1 [6] and stabilized index 2) did not show any significant differences. However, examples can be provided to show that careless error control for accelerations can lead to large errors in stress calculations, particularly in force methods.
9. The flexible system simulation methods in dynamics with the use of mixed FEM and MBS methods comprise an effective computational tool, especially if the systems being analyzed are composed of mechanisms which can be modelled as rigid bodies and a small amount of flexible bodies. A glider with landing gear is a good computational example of such a case.

This article is the last out of a series of papers going back into the mid-eighties [25], and several continuations from the nineties [11, 26].

References

1. Shabana, A.A., *Dynamics of Multibody Systems,* Wiley, New York, 1998.
2. Kane, T.R., Ryan, R.R., and Banerjee, A.K., 'Dynamics of a cantilever beam attached to a moving base', *AIAA Journal of Guidance, Control and Dynamics* **10**, 1987, 139–151.
3. Ambrosio, J., 'Geometric and material nonlinear deformation in flexible multibody systems', in *Proceedings* of the *NATO-ARW on Computational Aspects of Nonlinear Structural Systems,* Poland, 2000, 91–115.
4. Haug, E.J., *Computer-Aided Kinematics and Dynamics of Mechanical Systems, Volume I: Basic Methods*, Allyn and Bacon, Boston, 1989.

5. Garcia de J. and Eduardo B., *Kinematic and Dynamic Simulation of Multibody Systems*. Springer-Verlag, New York, 1994.
6. Brenan, K.E., Cambpell, S.L., and Petzold, L.R., *Numerical Solution of Initial Value Problems in DAE*. SIAM, Philadelphia, 1996.
7. Hairer, E. and Wanner, G., *Solving Ordinary Differential Equations II*, 2nd edn. Springer Verlag, Berlin, 1996.
8. Haug, E.J., Wu, S.C., and Yang, S.M., 'Dynamics of mechanical systems with coulomb friction, stiction, impact, and constraints addition, deletion. Part I, II, III', *Mechanism and Machine Theory* **21**, 1986, 401–425.
9. Armstrong-Helouvry, B. and Dupont, P., 'A survey of models, analysis tools and compensation methods for the control of machines with friction', *Automatica* **30**(7), 1994, 1083–1138.
10. Sohoni, V., *Joint Friction Modelling in ADAMS* 10.0. Draft, 2000.
11. Frączek, J., 'Dynamics of *mechanical systems with coulomb friction.* Part I. Theory', *The Archive of Mechanical Engineering* **XL**, 1993, 208–215.
12. Craig, R.R., 'Substructure methods in vibration', *Transactions of the ASME – Special 50th Anniversary Design Issue* **117**, 1995, 207–213.
13. McConville, J., Survey of FEA-Based Stress Methods in ADAMS – Aircraft Model Case Study, Internal MDI materials.
14. Schwertassek, R. and Wallrap, O., *Dynamics of Flexible Multi Body Systems,* Vieweg, Germany, 1999.
15. Claus, H., 'A deformation approach to stress distribution in flexible multibody systems', *Multibody System Dynamics* **6**, 2001, 143–161.
16. Yim, H.J., Haug, E.J., and Dopker, B., 'Computational methods for stress analysis of mechanical components in dynamic systems, in *Concurrent Engineering of Mechanical Systems*, Vol.1, Haug, E.J. (ed.), University of Iowa, Iowa City, 1989, 217–237.
17. Fischer, P. and Witteveen, W., Integrated MBS-FE-Durability Analysis of Truck Frame Components by Modal Stresses, *MDI Conference*, Rome, 2000.
18. Madej, J. (ed), '*The Technics of Rail–Road (Bimodal) Transport (in Polish) Research Institute of Rolling-Stock Industry', Poznań*, 2000.
19. Matej, J., Piotrowski, J., Wojtyra, M., and Frączek, J., 'Modelling and safety examination of the long bimodal train on curved track using ADAMS/RAIL', *Proceedings of the 1st MSC.ADAMS European User Conference (CDROM)*, Londyn, U.K., November, 2002.
20. Kik, W. and Piotrowski, J.P., 'A fast approximate method to calculate normal load at contact between weel and rail and creep forces during rolling', in *Proceedings of the 2nd Mini Conference on Contact Mechanics and Wear of Rail/Wheel Systems*, Ed. I. Zabory TU Budapest, 1996.
21. MSC.ADAMS 2003 Theory, – *Wheel–Rail Element Reference Guide,* MSC, 2003.
22. PW-6, Technical Documentation, DWLKK, Warsaw.
23. Frączek, J., *Modelling of Spatial Mechanisms Using Multibody Method*, WPW, Warsaw, 2002 (in Polish).
24. Żebrowski, J., 'Dynamical Analysis of PW-6 glider using MBS and FEM', MSc Thesis, Supervisor Frączek J. & A. Dacko.
25. Arczewski, K., 'Application of graph theory to the determination of kinetic energy of rigid body systems', *Journal of the Franklin Institute* **324**(3), 1987, 351–367.
26. Issa, S.M. and Arczewski, K., 'Wings in steady and unsteady ground effects', *Canadian Aeronautics and Space Journal* **44(3)**, 1998, 188–193.